JGR Oceans

RESEARCH ARTICLE
10.1029/2025JC022738

Field Observations of Sea Ice Thickening by Artificial Flooding

T. C. Hammer[1], L. L. van Dijke[1], A. Shestov[2], C. Haas[3,4], and H. Hendrikse[1]

[1]Faculty of Civil Engineering and Geosciences, Department of Hydraulic Engineering, Delft University of Technology, Delft, The Netherlands, [2]Arctic Technology Department, The University Centre in Svalbard, Longyearbyen, Norway, [3]Alfred-Wegener-Institute, Helmholtz Centre for Polar and Marine Research, Bremerhaven, Germany, [4]Institute of Environmental Physics, University of Bremen, Bremen, Germany

Abstract Arctic sea ice is retreating at a high rate, also due to the positive ice-albedo feedback loop: as ice melts and disappears, it reflects less sunlight, further accelerating ocean warming. One proposed way to slow the retreat is by thickening sea ice in winter, increasing its chances of surviving summer melt. This could be achieved by artificially flooding existing sea ice with seawater pumped from below, allowing it to freeze at the surface through exposure to cold air and thicken the ice layer. However, the effectiveness of this approach remains uncertain, as numerical models show contrasting results and few field experiments have been conducted. This study examines the growth and melt of ice through spring and summer after artificial flooding covering $\sim 1{,}500\ m^2$, resulting in thickened (+26 cm) snow-covered first-year sea ice. Observations were carried out in Vallunden Lagoon (Van Mijenfjord), Svalbard, from 20 March to 24 June 2024, with flooding and intensive in situ measurements from 11–15 April. Artificial flooding significantly heated the upper two-thirds of the original 90 cm thick ice, increasing salinity. Surface albedo evolution was influenced by specific events such as slush formation, snow drift, and a major meltwater drainage event in spring. Artificial flooding resulted in thicker ice and delayed rotten ice formation by 6 days, but did not delay the disappearance of ice in summer compared to a non-flooded reference site. Experiments at other scales and locations could help reveal how local conditions and flooded area size influence results and the potential of this method.

Plain Language Summary As Arctic sea ice melts and disappears, less sunlight is reflected from the Earth's surface, accelerating ocean warming. One proposed way to slow this process is to artificially thicken sea ice in winter, increasing its chance of surviving into summer while reflecting sunlight. This can be done by flooding ice with seawater when air temperatures are far below zero, allowing it to freeze at the surface and add thickness. However, the effectiveness of the method remains uncertain because few real-world tests have been performed. This study tested artificial flooding over $\sim 1{,}500\ m^2$ of sea ice in Svalbard in 2024 April, monitoring it remotely until 2024 June. Ice temperature, salinity, and solar reflection were measured before and after flooding. The results show flooding warmed most of 90 cm thick ice and allowed salty water to soak in. Events such as snow drift, slush, and a major spring drainage affected how much sunlight the surface reflected. Although flooding produced thicker ice (+26 cm) and delayed rotten ice formation by 6 days, it did not make the ice last longer in summer than nearby non-flooded ice. Tests at other scales and locations could reveal how local conditions and flooded area size influence results.

Key Points:

- A field campaign in Svalbard used artificial flooding to investigate sea ice thickening in the context of geoengineering
- Flooding an area of $\sim 1{,}500 m^2$ resulted in 26 cm of snow ice, increased ice temperature and salinity, and affected surface albedo evolution
- The snow ice layer delayed rotten ice formation by 6 days but did not extend sea ice survival for scale and location of this experiment

Supporting Information:

Supporting Information may be found in the online version of this article.

Correspondence to:

T. C. Hammer,
t.hammer@tu-braunschweig.de

Citation:

Hammer, T. C., van Dijke, L. L., Shestov, A., Haas, C., & Hendrikse, H. (2026). Field observations of sea ice thickening by artificial flooding. *Journal of Geophysical Research: Oceans*, *131*, e2025JC022738. https://doi.org/10.1029/2025JC022738

Received 14 APR 2025
Accepted 20 MAR 2026

Author Contributions:

Conceptualization: T. C. Hammer, L. L. van Dijke, H. Hendrikse
Data curation: T. C. Hammer, L. L. van Dijke, A. Shestov, H. Hendrikse
Formal analysis: T. C. Hammer, C. Haas, H. Hendrikse
Funding acquisition: L. L. van Dijke, H. Hendrikse
Investigation: T. C. Hammer, L. L. van Dijke, A. Shestov, H. Hendrikse
Methodology: T. C. Hammer, L. L. van Dijke, A. Shestov, H. Hendrikse
Project administration: T. C. Hammer, L. L. van Dijke, A. Shestov, H. Hendrikse
Resources: A. Shestov
Software: T. C. Hammer, H. Hendrikse

1. Introduction

The extent of sea ice in the polar regions is declining rapidly, with Antarctic sea ice reaching a record low in 2023 (Gilbert & Holmes, 2024) and a decadal trend of sea ice decline of 13% in the Arctic (Yadav et al., 2020). The melting of Arctic sea ice causes a positive feedback mechanism associated with a reduction in albedo. Albedo, a measure of the reflected shortwave radiation from the surface of the Earth, decreases as sea ice area decreases and makes space for open water, leading to increased energy absorption by- and warming of the ocean. This, in turn, accelerates the melting of sea ice giving rise to a feedback loop. This feedback loop is a key factor contributing to the significant rise in air temperatures in the Arctic, a phenomenon known as Arctic Amplification.

One proposed geoengineering method aiming to counter or delay this decline of sea ice extent is to thicken sea ice by means of artificial flooding. The ability of the ice to survive through the summer could be enhanced by freezing additional ice layers onto the existing sea ice when air temperatures are still far below freezing. The longer surviving ice then reflecting more solar radiation compared to open ocean makes this an example of solar

Supervision: T. C. Hammer, H. Hendrikse
Validation: T. C. Hammer, L. L. van Dijke, A. Shestov, C. Haas, H. Hendrikse
Visualization: T. C. Hammer, A. Shestov
Writing – original draft: T. C. Hammer
Writing – review & editing: T. C. Hammer, L. L. van Dijke, A. Shestov, C. Haas, H. Hendrikse

radiation management also referred to as surface albedo modification. Solar radiation management has been widely discussed in the context of Arctic sea ice geoengineering (Field et al., 2018; Pauling & Bitz, 2021; Webster & Warren, 2022; Zampieri & Goessling, 2019). There is, however, limited information on the physical viability of such geoengineering methods as execution of larger field trials continues to be subject of intense debate and requires regulatory frameworks to be in place (Siegert et al., 2025).

Artificial flooding of sea and lagoon ice has a long history in engineering. Historically, sea ice was flooded to increase the thickness and strength of floating ice platforms, grounded ice islands, and ice roads (Barrette, 2015; Cox, 1979; Karelov et al., 2015). In general, the focus was on aspects related to ice engineering (e.g., ice strength and bearing capacity) during the cold season rather than on melt season processes (Barrette, 2015; Masterson, 2009). The ice was typically prepared prior to flooding, something that is impractical at the scales associated with the polar regions sea ice extent. For example, snow thicker than 5–15 cm was removed (Baudais et al., 1976) leaving low snow-to-ice thickness ratios. The low snow-to-ice thickness ratio leads to increased positive freeboard (i.e., the height of the ice surface above the waterline) before the thickening of the ice. Thus, after successful ice thickening the new ice surface sloped downwards away from the center of flooding if local and stationary flooding was performed (Nakawo & Frederking, 1981). Typically, two types of controlled (here: artificial) flooding are differentiated: Constrained- and free-flooding (Cox, 1979). The former method includes the construction of confinements (e.g., snow dams) to confine the water during flooding. The latter method does not consider any intervention to constrain the flooded water.

The impossibility to remove snow at a large scale makes the application of artificial flooding for sea ice thickening in the context of geoengineering have a lot in common with natural flooding events. Natural flooding occurs mainly when the ice freeboard is negative. This happens when ice layers are pushed below the water level by loading. Mostly, loading is caused by thick snow (Rösel et al., 2018), but can also be caused by other mechanisms like pressure ridge formation (Lewis et al., 2011; Massom et al., 1997). The negative freeboard can initiate relatively rapid lateral or vertical intrusion of seawater (Ackley et al., 2020; Lewis et al., 2011; Perovich et al., 2004; Provost et al., 2017). Once the snow is flooded, a slush layer forms, which transforms into snow ice when freezing (i.e., solidifying). Other types of natural flooding occur through upward percolation of brine (Eicken et al., 1995; Golden, 2001; Lewis et al., 2011; Provost et al., 2017), or the percolation of snow melt water or liquid precipitation (Fichefet & Morales Maqueda, 1999; Haas et al., 2001; Pauling & Bitz, 2021; Saloranta, 2000). Natural flooding can also be caused by wave-ice interaction or break-up events in zones of higher ice pressure, changing the isostatic equilibrium of ice floes temporally (Itkin et al., 2017; Lewis et al., 2011; Massom et al., 2001; Provost et al., 2017). Like artificial flooding, natural flooding affects the thermal insulation, ice permeability, ice mass balance, and the climate feedback of sea ice (Ledley, 1991; Maksym & Jeffries, 2001).

When applying artificial flooding for geoengineering purposes a large portion of the thickened ice would consist of snow ice since snow removal is not feasible at that scale. In studies on artificial flooding, snow ice was often reported to be "bonded firmly" to the original sea ice layer (Masterson, 2009). However, laboratory experiments performed by Jutras et al. (2016) showed that depending on slush thickness, salinity and temperature, ice crystals start floating in the slush layer, creating a liquid layer at the interface between the slush and original ice layer. According to Jutras et al. (2016), such events of high saline layer separation could be caused by a strong snow storm in nature and have been documented in earlier reports as wet conditions and *gap layers* at the snow-ice/ice interface (Haas et al., 2001; Lytle & Ackley, 1996; Meguro, 1962). The main differences in the interface conditions might thus be explained by different thicknesses of snow and slush, and the amount of water added in a single flooding event. The salinity of snow ice formed after artificial flooding is often found to be relatively high (i.e., 20–30 ppt) in comparison to the salinity of the original sea ice (Baudais et al., 1976). In the following, we refer to the original sea ice as interior ice.

This study addresses the question of the effectiveness of using artificial flooding without snow removal, or other forms of preparation of the ice surface, to create thicker ice with the purpose of extending the survivability of the ice in summer. A field experiment was conducted in the Arctic using flood pumps to perform the intervention on snow-covered first-year sea ice, followed by monitoring ice growth and the subsequent melting of the thickened ice. The analysis uses in situ measurements collected during a field campaign, and continuous, autonomous measurements covering the sea ice evolution until disappearance in summer. The chosen flooding approach, the scale, and the site-specific conditions related to the field tests are discussed in the context of the application of artificial flooding for geoengineering purposes. The comparison to natural flooding events is also reflected upon.

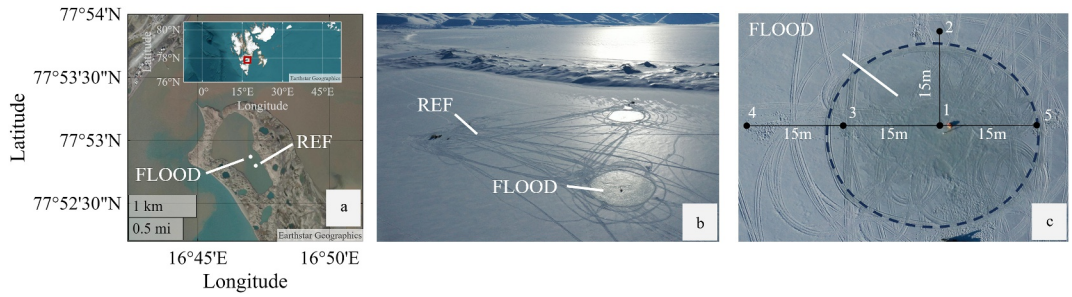

Figure 1. Aerial views of the flooding experiment in the Vallunden lagoon, Svalbard. (a) Satellite image of the Vallunden lagoon with its location on Svalbard shown in the inset. (b) Drone image from 12 April showing the reference site (REF) and flooded site (FLOOD) after the first flooding event. (c) Top-down view of Site FLOOD indicating ice-coring locations and horizontal distances between cores.

2. Method

This study uses field data of artificial flooding of snow-covered first-year landfast sea ice in the Vallunden Lagoon (Figure 1). A narrow inlet connects the lagoon with the Van Mijenfjorden. The lagoon is thus protected from incoming swell. The lagoon is shallow (average depth of 10–11 m) and has a size of roughly 0.5 to 1 km^2. Its water column is well mixed by tidal currents (Morozov et al., 2019). The data were obtained between 10 April and 24 June 2024. On 24 June all measurement stations collapsed due to loss of integrity of the supporting ice. The data are publicly available (Hammer et al., 2024a) and are described in detail in Hammer et al. (2024b).

Here we analyze the data from two out of four test sites that were instrumented in the field (Figure 1b). In Hammer et al. (2024b) further information on the conditions, equipment and flooding activities at the reference test site, Site REF, and the artificially flooded test site, Site FLOOD and two other sites (i.e., site C [FLOOD1] and D [FLOOD2]) can be found. Site FLOOD1 and FLOOD2 were used for testing flooding strategies focusing on the engineering aspects of flooding and are not further described here.

2.1. Conditions at the Sites Prior to Flooding

The conditions on the test sites before flooding are summarized in Table 1, including median air temperature $T_{air,med}$, mean interior ice top surface temperature $T_{ice,mean,top}$, mean interior ice bottom surface temperature $T_{ice,mean,bot}$, median ocean temperature $T_{ocean,med}$, median diffusivity proxy for the air $\beta_{air,med}$, ice $\beta_{ice,med}$, and ocean layer $\beta_{ocean,med}$, mean snow thickness $h_{snow,mean}$, mean interior ice thickness $h_{ii,mean}$, and daily averaged albedo α_d. The diffusivity proxy β is calculated as the linear approximation of the thermal diffusivity (Jackson et al., 2013; Provost et al., 2017). The data source and number of ice cores or snow samples (No.) used for obtaining statistical measures are indicated in Table 1.

The initial temperature profiles of the interior ice at Site FLOOD and Site REF were linear, increasing from −9.0°C to −8.3°C at the ice top surface to −2.3°C to −2.2°C at the ice–ocean interface. Note that the probe was inserted a few centimeters into the bottom of the ice core to avoid recording air temperature. Snow thickness

Table 1
Conditions on the Test Sites on 11 April Prior to Artificial Flooding

Site	Date[a]	$T_{air,med}$	$T_{ice,mean,top}$ (*No.*)	$T_{ice,mean,bot}$ (*No.*)	$T_{ocean,med}$	$\beta_{air,med}$	$\beta_{ice,med}$	$\beta_{ocean,med}$	$h_{snow,mean}$ (*No.*)	$h_{ii,mean}$ (*No.*)	α_d
		°C	°C	°C	°C	–	–	–	*cm*	*cm*	–
FLOOD	20.03	−15.8[b]	−9.0 (5)[c]	−2.3 (5)[c]	−1.88[b,d]	1.08[e]	1.02[e]	1.03[e]	17 (8)[f]	90 (10)[f]	0.74
REF	10.04	−14.8[b]	−8.3 (1)[c]	−2.2 (1)[c]	−1.88[b,d]	1.12[e]	1.02[e]	1.00[e]	15 (6)[f]	90 (6)[f]	0.72

[a]Date of installation of autonomous measurement equipment. [b]Time-averaged autonomous air temperature measurements recorded from 08:00 to 15:30 on 11 April (Snow Ice Mass Balance Apparatus [SIMBA]). [c]Depth-averaged in situ ice core temperature measurements. [d]Corrected for accuracy of measurement (±0.0625°C). [e]Depth-averaged autonomous diffusivity proxy calculated per layer (SIMBA). [f]In situ snow thickness measurements.

ranged from 15 to 17 cm, and the interior ice was approximately 90 cm thick at both sites. The diffusivity proxy of the interior ice remained essentially constant at 1.02, distinguishing it from air, snow, and seawater. The initial daily averaged albedo was 0.72 at Site FLOOD and 0.74 at Site REF.

2.2. Artificial Flooding

The artificial flooding was conducted using ice road pumps (Erikssons Mekaniska Verkstad AB) which were installed in pre-drilled holes in the sea ice without any further preparation of the sea ice or snow cover. This approach is consistent with the envisaged application of flooding in the context of geoengineering. The pumps drew water directly from below the ice, the water having a temperature very close to the freezing point (i.e., $T_{water,flooded} \approx -1.9°C$). The water was then released in the form of a jet of water onto the snow-covered sea ice. Site FLOOD was flooded on 11 April from 17:30 to 18:45 at a rate of 3,500 $\mathrm{L\,min^{-1}}$. The site was flooded a second time on 12 April from 17:10 to 19:00. The approach to flooding is further analyzed in Section 3.1 and discussed in Section 4.2.

On 12 April weather conditions allowed to operate a drone in the area to collect areal footage from the flooded site (Figures 1b and 1c). A brief analysis on the flooded area is included here. On 11 April the pump on Site FLOOD was running for 75 min at its maximum discharge rate of 3.5 $\mathrm{m^3 min^{-1}}$ resulting in an expected flooded area of 1,458 $\mathrm{m^2}$ when accounting for the snow layer of ∼20 cm thickness to be fully saturated and assuming an initial water content of 10%. Drone footage taken after flooding, which can be found in Supporting Information S1, showed a wet snow surface over a visible radius r_1 of ∼20 m. The value was derived from a photogrammetric analysis of the field after flooding resulting in a wet area of 1,217 $\mathrm{m^2}$ (i.e., 19.7 m radius). The Agisoft Metashape software was used to generate a georeferenced 3D model, which enables the measurement of areas once a polygon is defined. The polygon boundaries were based on visually distinguishable features in the images, which were also clearly represented in the 3D model.

The detected area is about 83% of what was expected based on the volume of water pumped onto the ice. The remaining 17% are believed to have been missed by the drone, as slush also formed below the snow surface at the edges of the flooded area and was therefore not visible. Additionally, water might have been lost through vertical drainage, through brine inclusions or cracks. Unfortunately, poor weather did not allow to capture drone footage after the second flooding of site FLOOD on 12 April. Normalized difference water index layer imagery from the Sentinel 2 satellite suggest a total diameter of ∼28 m of the flooded area after the second flooding (Hammer et al., 2024b). Further, it was observed that the majority of the water ran off and extended the radius of the slush layer instead of increasing the (snow) ice thickness. Estimating that the second flooding event primarily flooded the surrounding snow, rather than increasing the (snow) ice thickness of the previously flooded area, the flooded distance would be 29.3 m. The thermistor chain embedded in the ice approximately 30 m away from the center of flooding did not show any temperature changes after the second flooding, indicating that the water had not traveled to that location.

2.3. Measurements

The measurements conducted to study the growth and melt of ice before, during, and after the artificial flooding are described in this section. Four types of measurements are distinguished. The first are the continuous autonomous measurements resulting in vertical temperature profiles. Second are the continuous autonomous surface albedo measurements used to study the reflectivity of the ice. Third are the in situ measurements taken from ice coring which served to obtain an insight in the spatial distribution of the effects of flooding right after the flooding was performed. Finally, surface photographs were taken with a time-lapse camera left in the field. An overview of all physical quantities measured for the two sites of interest is provided in Table 2. A close up on one of the installed wooden poles and attached measurement systems can be found in Figure 9 of Hammer et al. (2024b).

2.3.1. Vertical Temperature Profiles

The SIMBA installed at the center of each test site was used to obtain temperature profiles and to extract data for detection of the boundaries between different layers of air, snow, slush, ice, and water and their evolution over time. Temperature measurements were conducted at intervals of ±2 cm along a 5 m long thermistor chain which

Table 2
Measurements Taken During the Study

Autonomous measurements	Site
Vertical temperature profiles	REF, FLOOD
Incoming and reflected short- and long-wave radiation on the surface of the ice	REF, FLOOD
Wind direction, wind speed, and atmospheric pressure	FLOOD
Surface photographs	REF, FLOOD
In situ measurements	
Ice coring	REF, FLOOD

was installed in the ice of about 90 cm thickness, and extended above into the air and below into the water. Throughout the measurement period the sampling rate was varied to adapt to variation in the relevant time scale of temperature change. The sampling rate was 6 hours for the period between 20 March and 10 April, 15 min around the times of flooding between 11 and 23 April, and 2 hours during the remote monitoring phase between 23 April and 24 June. The sensors along the thermistor chain were periodically heated ($t_{cycle} = 24$ hrs) in order to aid detection of the boundaries between the different layers with different thermal properties (Jackson et al., 2013; Provost et al., 2017).

2.3.2. Surface Albedo Measurement

The effect of artificial flooding on the evolution of surface albedo was monitored with the radiometers on Site FLOOD and Site REF. From the measurements, the mean daily surface albedo α_d was calculated from the instantaneous incident radiation values as:

$$\alpha_{\mathrm{d}} = \frac{SW_{\uparrow}^{\mathrm{sfc}}}{SW_{\downarrow}^{\mathrm{sfc}}} \tag{1}$$

with $SW_{\downarrow}^{\mathrm{sfc}}$, the daily averaged instantaneous incident shortwave radiation near the surface as obtained with the upward looking pyranometer, and $SW_{\uparrow}^{\mathrm{sfc}}$, the daily averaged instantaneous reflected shortwave radiation at the surface obtained with the downward looking pyranometer. Night-time values were set to zero and the transition between day and night was calculated based on the solar elevation angle (Kopp, 2023).

2.3.3. Ice Coring

Ice cores were taken, before, during and up to 4 days after artificial flooding (10–15 April) with the aim of investigating the spatial distribution of water after flooding, the subsequent growth of snow ice, and for validation of the layer detection with the automated SIMBA-based procedure. In total, 57 ice cores were collected across both test sites.

The coring locations were based on a coring pattern as shown in Figure 1c. The orientation of the coring pattern was defined with respect to the location of the pump and direction of pumping during the first flooding per test site. The coring pattern on Site REF was copied from Site FLOOD. For documentation purposes a reference system for the ice cores was introduced. The zero vertical coordinate was set to coincide with the top surface of the interior ice layer which is defined here as the ice layer present prior to flooding. Any additional ice (e.g., snow ice) and snow thus have a negative vertical coordinate.

At least two ice cores were retrieved per sampling location with the purpose of obtaining ice temperature, bulk salinity, bulk density, snow depth and freeboard. The first ice core was transported immediately after retrieval to the field measurement station on the site, where temperature measurements were immediately conducted to minimize cooling of the ice core. Ice temperature was measured in increments of 5 cm along the length of the core by drilling into it and inserting a thermometer probe. The measurements were taken as replicate measurements in case the SIMBA thermistor chains should fail, to gain insight into the spatial variability of temperature, and to have reference data for the salinity and density measurements. Bulk salinity was obtained from measurements of

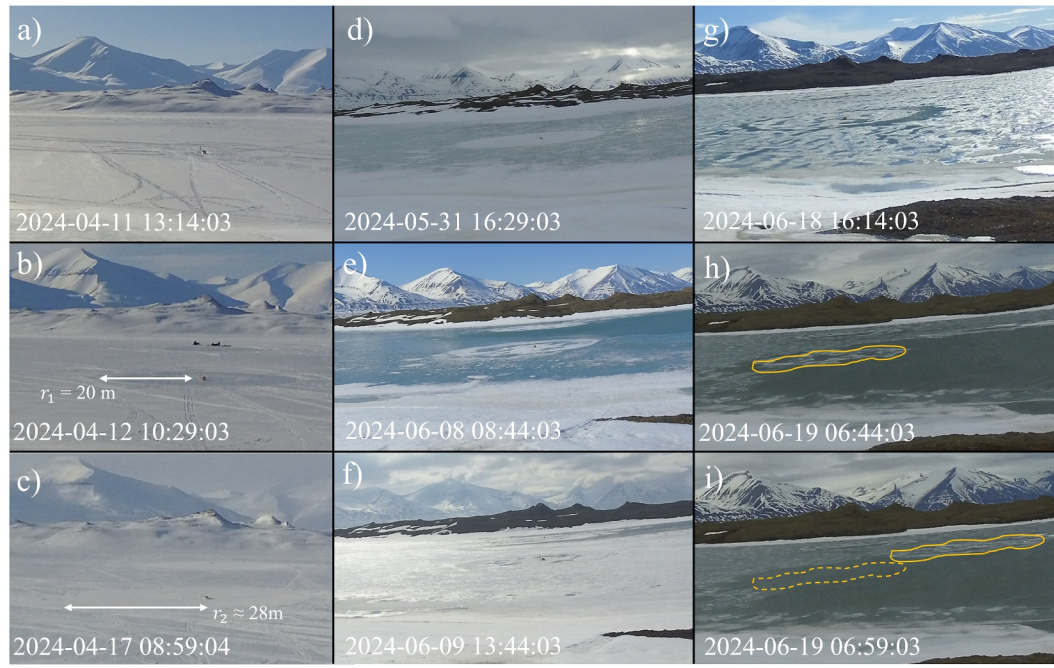

Figure 2. The sequence of identified relevant events at Site FLOOD, detailing the evolution of the thickened sea ice from its initial state prior to flooding (a) through flooding (b, c), melting (d–g), and eventual disintegration (h, i). The radius of the visibly flooded circle after the first (r_1) and second flooding (r_2) event are provided. The yellow lines indicate the current ice floe position after separation (solid, panel h) and the initial position (dashed, panel i).

the conductivity of 10 cm long sections of the ice core melted in plastic bags inside a heated cabin. The reader is referred to Hammer et al. (2024b) for further information on the measurement equipment and visualization of the experimental design, materials, and methods.

2.3.4. Surface Photographs

To obtain visual information about the evolution of sites REF and FLOOD a time-lapse camera was installed on the mountain ridge in the North-East such that it oversaw most of the lagoon and was left recording in the field until summer. Photographs obtained with the camera are used for event detection in the present study; a time-lapse movie covering the entire period between April and June can be found in the data repository (Hammer et al., 2024a).

3. Results

The results are presented chronologically, focusing on eight key surface events at Site FLOOD. Figure 2 provides an overview of these events (b–i) captured by the time-lapse camera, including the initial conditions (a) described in Section 2.1. Table 3 lists the corresponding time periods and related internal ice processes. The diffusivity proxy, derived from temperature and heat cycle measurements, is displayed in Figure 3. The local mean albedo, calculated from the radiometer data, is shown in Figure 4. The derived evolution of interior ice thickness is illustrated in Figure 5. Meteorological data (e.g., wind speed, direction, and pressure) are available in Hammer et al. (2024b) but are not discussed here.

3.1. (b)–(c) Flooding and Snow Drift

The following paragraphs describe in detail the evolution of temperature, salinity, snow salinity, and surface albedo during the flooding period. In short, the following main observations have been made up to 95 hrs after the first artificial flooding:

1. The mean temperature of the interior ice layer increased between 2.4 and 2.7°C.
2. An increase in ice permeability caused salt intrusion into the upper interior ice layer.

Table 3
Chronological Sequence of Observed Surface and Internal Processes

Date	Event	Surface processes	Internal processes
11 April (see Table 1)	a	Initial conditions	–
12 April	b	A dark patch (slush) marks the flooded area	Slush starts freezing
15 April	–	–	Upper slush layer transforms to snow ice
17 April	c	Bright snow has drifted onto the site	Bottom slush layer transforms to snow ice
18 April	–	–	A porous layer begins to form below the top surface of the interior ice
30 April	–	–	Rotten snow ice forms at the depth of the former upper slush layer reforms
7 May	–	–	Rotten snow ice forms at the depth of the former bottom slush layer
31 May	d	The snow cover has disappeared	One single layer of rotten snow ice forms
8 June	e	Meltwater surrounds the site	–
9 June	f	Following a major meltwater drainage event, a bare ice layer surrounds the site	False bottom formation
18 June	g	Small melt ponds and a circular melt trench develop around the site	–
19 June	h	The rotten ice starts drifting as a detached ice floe	–
19 June	i	The ice floe comes to rest after drifting for approximately 15 min	–
20 June (see Table 5)	–	Disappearance of the rotten ice	–

Note. Surface processes correspond to the events labeled in Figures 2a–2i, while internal processes describe transformations within the ice and slush layers based on observations in Figure 3.

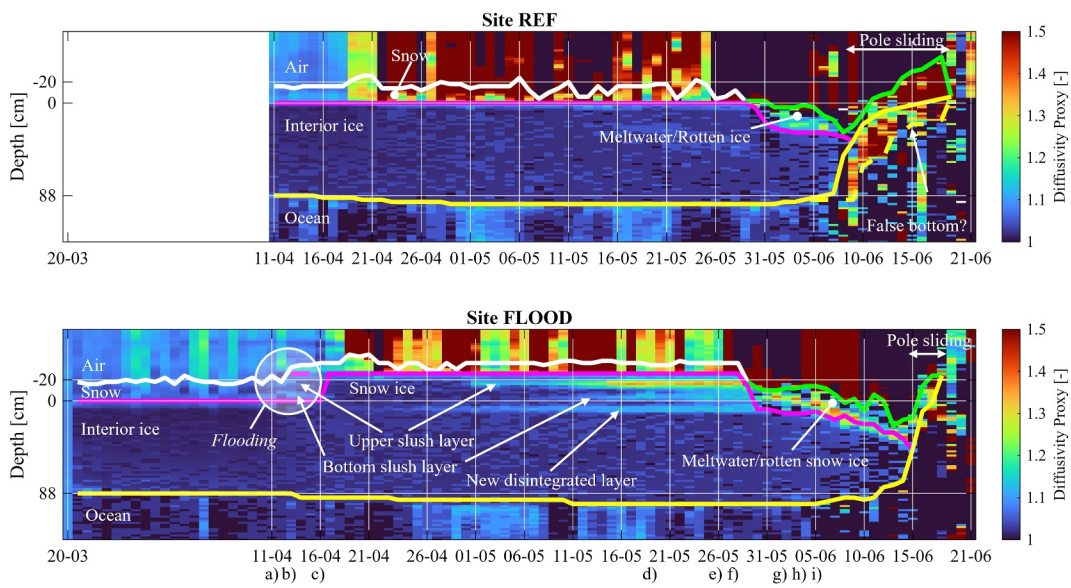

Figure 3. The thermal diffusivity proxy was used to aid manual identification of the snow ice and interior ice layers on Site REF and Site FLOOD. The white lines show the snow surface, the pink lines show the ice surface. The yellow lines show the bottom of the interior ice. The green lines show the surface of the rotten snow and interior ice (Site REF), and rotten snow ice (Site FLOOD), respectively. In late spring, the measurement pole starts sliding into the rotten ice, making the green and yellow lines start rising.

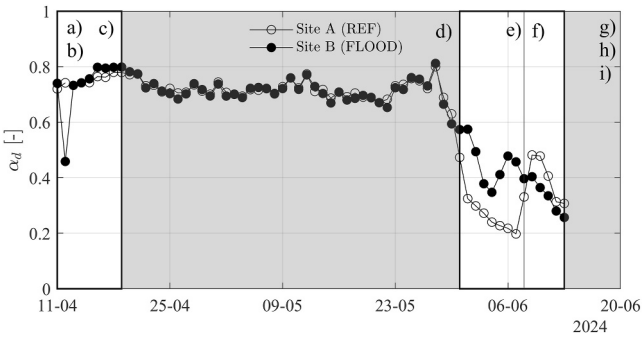

Figure 4. Mean daily surface albedo α_d on Site FLOOD and Site REF for the measurement period from 11 April to 13 June.

3. The thickened ice became snow covered again due to redistribution of drifting snow.

The flooding experiment caused an immediate rise in the snow layer temperature at Site FLOOD, evident from the two distinct warm zones in the vertical temperature profile (Figure 7). These warm zones indicate the formation of a transient hydrostatic water reservoir around the thermistor chain that subsequently froze, forming an ice bustle around the pole (see also Hammer et al. (2024b)).

The ice top surface temperature ($T_{\text{ice,mean,top}}$) increased roughly 42 hrs after first flooding by up to 5.9°C (see Table 4). On average, ice temperature increased between 2.4 and 2.7°C along the depth of the interior ice layer ($T_{\text{ice,mean,int}}$) for the same time period. More specifically, the flooding caused a warming of approximately two-thirds of the upper interior ice layer (0–60 cm along the vertical axis—Figure 6, left). Only the bottom third part of the interior ice remained unaffected (60–90 cm along the vertical axis). The temperature profile had not recovered 95 hrs after the first flooding event. The flooding on Site FLOOD did not affect the temperature measurements on Site REF, which shows that the sites were sufficiently far apart for independent analysis.

By 17 April, it becomes difficult to visually distinguish the flooded snow layer from the interior ice layer based on the vertical temperature profile in Figure 7. The same holds for the diffusivity proxy (Figure 3). The slush layer thus fully transformed into snow ice yielding a diffusivity proxy similar to the interior ice.

When mean air temperatures began rising substantially 1 week after flooding (i.e., 19 April at 9:00: $T_{air} = -0.5°$), marking the onset of the melting season, the temperatures of the interior ice still had not recovered from the warming caused by the artificial flooding.

Prior to flooding, the salinity profile at Location 2 showed high values at the ice–ocean interface (~8.3 ppt) compared to the interior average (4.5 ppt—Figure 6, right). After flooding, the interior ice salinity significantly increased in magnitude showing a linear profile from the top (~7 ppt) down to ~30 cm depth (4.8 ppt). Furthermore, a highly saline layer (14–15 ppt) formed at the slush-interior ice interface.

The salt intrusion extended down to ~30 cm, coinciding with the critical permeability threshold introduced by Golden (2001). According to Golden, interior ice becomes permeable when temperatures exceed −5°C (for 5 ppt salinity); this critical isotherm was exceeded to 30 cm depth 24 hrs post-flooding (Figure 6, left), allowing highly saline slush brine to migrate into the interior ice. As temperatures later recovered, core salinity decreased while surface and bottom values increased, indicating partial salt expulsion.

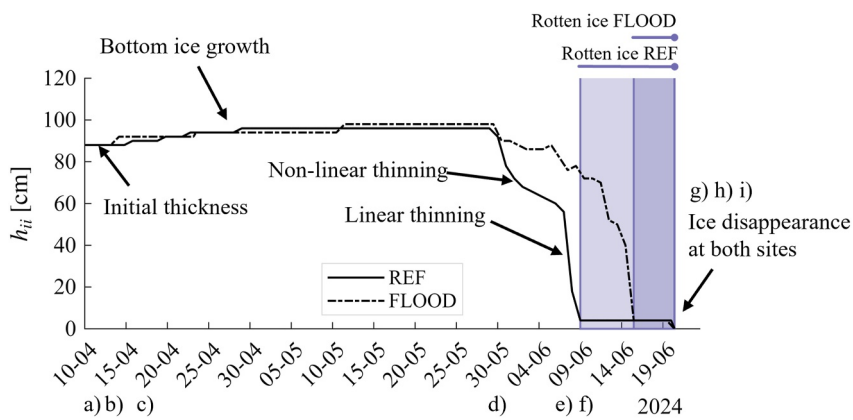

Figure 5. The determined interior ice thickness h_{ii} for the two test sites. The purple lines indicate the period during which the majority of the interior ice has transformed into rotten ice. The rotten ice layer disappears almost instantly given the time scale of the processes considered. The values presented have an uncertainty of ±4 cm.

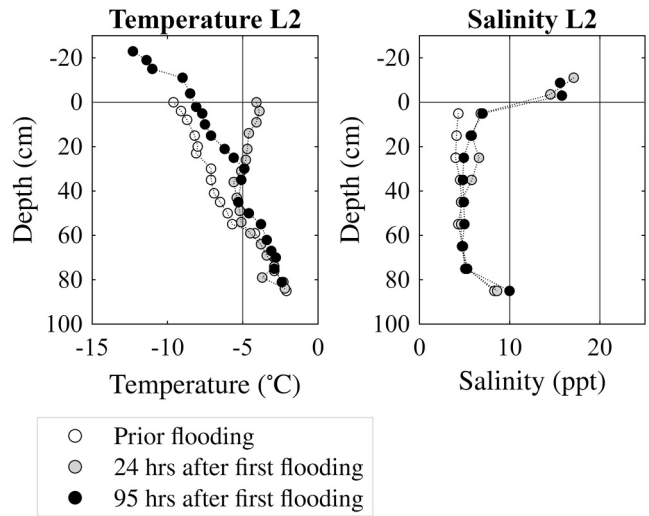

Figure 6. Vertical core profiles of temperature and salinity on Site FLOOD for Location 2 (i.e., in 15 m distance to the measurement station and center of the flooding, Figure 1c) for three different dates.

The snow layer, re-established by drifting of snow, became highly saline on 16 April (~22.7 ppt at Location 1, Site FLOOD), exceeding consolidated snow ice salinity. Takizawa (1985) attributes this to brine *wicking* via capillary suction, with Massom et al. (1997) noting saline frost flower incorporation into snow; also observed in our experiments (Supporting Information S1). Nakawo and Frederking (1981) also reported that ~half of the salts were "lost" during the freezing process. The high snow salinity indicates that these losses are related to brine being expelled to the ice surface.

The flooding temporarily reduced the surface albedo by about 40%, from $\alpha_d = 0.8$ to $\alpha_d = 0.5$ (Figure 4), due to the darker flooded surface relative to the original snow cover (Figures 1c and 2b). However, the flooded area became covered by ~10 cm of snow again within 24 hrs after the second flooding, restoring the albedo by 13 April (Figure 4). Shortly thereafter, the mean daily albedo at Site FLOOD not only recovered but exceeded that of the reference site (Figure 2c), likely because the snow at Site REF had begun to melt and formed a snow crust, which can reduce albedo by 1%–10% compared to fresh snow (Manninen et al., 2021). A subsequent short snowfall on 19 April, followed by strong winds (gusts up to 20 m s^{-1}), deposited a thin (<4 cm) snow layer that equalized albedo at both sites.

3.2. (c)–(d) Snow Ice Formation and Melt

This section examines the post-flooding period (12 April–30 May), when sea ice thickened via snow ice formation, which later melted. Analysis relies on automated measurements. Key observations span 4–50 days after initial flooding at Site FLOOD:

Table 4
Conditions on Site FLOOD and Site REF on 11 April prior Flooding and on 13 April, 42 hrs After Flooding

	Ice top surface		Ice bottom surface		Interior ice	
	prior	*after*	*prior*	*after*	*prior*	*after*
	$T_{ice,mean,top}$ (°C)	$T_{ice,mean,top}$ (°C)	$T_{ice,mean,bot}$ (°C)	$T_{ice,mean,bot}$ (°C)	$T_{ice,mean,int}$ (°C)	$T_{ice,mean,int}$ (°C)
FLOOD	−9.0 (5)[a]	−3.1 (1)[b]	−2.3 (5)[a]	−2.4 (1)[b]	−6.0 (5)[a], −6.5[c]	−3.7 (1)[b], −3.8[d]
REF	−8.3 (1)[a]	−8.1 (6)[e]	−2.2 (1)[a]	−2.3 (6)[e]	−4.6 (1)[a], −4.1[c]	−4.5 (6)[e], −4.7[d]

Note. Numbers of ice cores used for analysis are given in parentheses. Temperatures for the interior ice are depth-averaged over the thickness. [a]In situ ice core temperature measurements from 11 April. [b]In situ ice core temperature measurements on Location 1 from 13 April. [c]Autonomous ice temperature from 11 April at 15:30 (SIMBA). [d]Autonomous ice temperature from 13 April at 11:15 (SIMBA). [e]In situ ice core temperature measurements from 11 to 15 April.

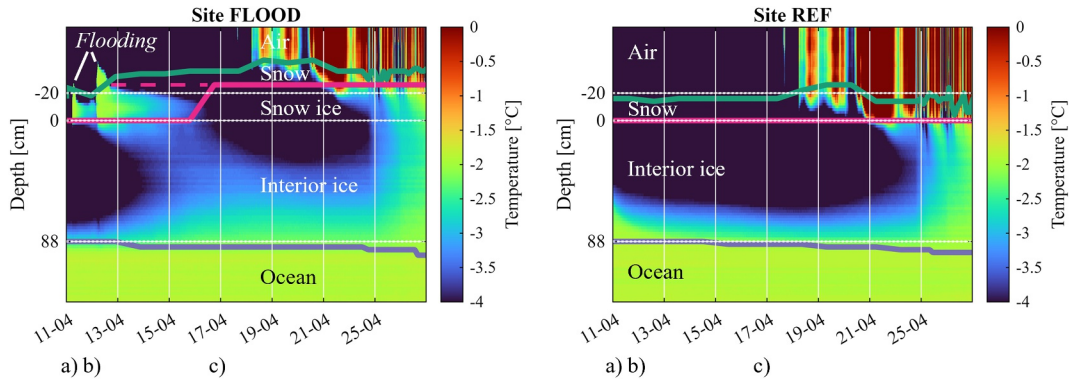

Figure 7. Temperature profiles around the time of flooding recorded with the Snow Ice Mass Balance Apparatus on Site FLOOD and Site REF. The green lines show the snow surface. The magenta lines show the snow ice and the interior ice surface, respectively. The purple lines show the bottom of the interior ice. The dashed magenta line marks the initial snow ice formation, when the layer had not yet fully solidified.

1. A snow ice layer formed at an averaged rate of 2.3 mm h^{-1}.
2. The snow ice layer of 26 cm total thickness had no significant effect on the basal growth of the interior ice with a thickness of 90 cm.
3. The snow ice layer melted at a rate of 5.4 mm h^{-1}.

The flooding of the snow, followed by freezing, resulted in the formation of a snow ice layer with a thermal diffusivity proxy similar to that of the interior ice (i.e., $\beta_{proxy} = 1.02$) (Figure 3). The averaged growth rate of the snow ice was 2.3 mm h^{-1} using the time instance after the last flooding event and the time instance when the full layer obtained a diffusivity proxy of 1.02 (i.e., from 12 April-19:00 to 17 April-10:30). The snow ice formed at an average air temperature of −15°C (including day and night) and with mean wind speeds around 10 m s^{-1}. Interestingly, the snow ice formed both from the top and the bottom of the flooded snow layer. Flooding the site twice over a relatively short time period of about a day, effectively created three to four freezing surfaces. Two slush layers were found separated by a 4–5 cm thick snow ice layer that formed after the first flooding, as can be seen in the data (Figure 3). The final snow ice surface exceeded the initial snow surface by only 6 cm. This is a result of the choice of free-flooding, which increased the radius of the flooded area rather than its thickness when the snow ice surface is flooded a second time.

Already from 18 April onward, the solidified snow ice layer started to degrade. First a porous internal layer started to develop, then both slush layers reformed on 30 April and on 7 May, and by 30 May all three slush layers, and the meltwater of the snow, had merged into a single warm, highly porous rotten snow ice layer. Interestingly, the thermal diffusivity proxy below the snow ice layer remained largely unaffected by the increase in air temperatures (i.e., the interior ice remained solid). Only the former top surface of the interior ice showed signs of transformation, while the bottom surface exhibited basal growth. The transformation at the top surface of the interior ice is considered to be caused by the warming of the top surface and subsequent salt migration into the interior ice.

The basal growth on Site FLOOD was found similar to the basal growth observed at Site REF (see Figure 5). This means that the additional snow ice layer of 26 cm total thickness had no significant effect on the basal growth. It remains unknown if this effect is caused by a combination of reduced snow insulation and warming of the majority of the interior ice, by the unaffected bottom temperature of the flooded interior ice, or simply by the inaccuracy of the layer detection and small magnitude of basal growth due to the late flooding in the season.

Eventually, the snow ice layers on all test sites melted almost simultaneously after 29 May, with a linear thinning of 5.4 mm h^{-1}.

3.3. (d)–(f) Drainage and First Melting

This section focuses on the time period after snow (ice) melt (30 May) until the occurrence of a massive drainage event on 8 June. Varying diffusivity proxy located between the ocean and air layer are referred to as rotten snow

ice or rotten interior ice, respectively based on the distinguishable diffusivity proxies (see Table 1 and Figure 3). In short, the following main observations have been made between 50 and 60 days after the first flooding:

1. Meltwater on Site REF reduced the albedo significantly, when compared to the exposed rotten snow ice on Site FLOOD.
2. A massive drainage event reversed this albedo difference between the two sites.
3. The interior ice at the flooded site shows a non-linear thinning, with a low initial rate which increased toward the end of the period.

Different surface textures on Site FLOOD and Site REF are visually recognizable after the snow melt on 30 May (Figure 2d). On Site FLOOD a whitish surface (i.e., rotting snow ice) is visible with the contours of the flooded area. On Site REF, meltwater is visible. The meltwater could not accumulate on Site FLOOD as its surface was higher at the moment of the onset of melting when compared to Site REF (see Figure 3). The different materials at the surface of both sites also led to the differences in mean daily albedo obtained for this period: Site FLOOD (i.e., the rotten snow ice) shows nearly twice the albedo ($\alpha_{d_{FLOOD}} = 0.4$–0.6) compared to the meltwater on Site REF ($\alpha_{d_{REF}} = 0.2$–0.3) (Figure 4).

However, on 8 June, this difference in the albedo for the sites inverts: $\alpha_{d_{FLOOD}}$ decreases to 0.25–0.4, while $\alpha_{d_{REF}}$ increases to 0.3–0.5. Site REF appears to have experienced a significant meltwater drainage event, as can be seen from comparing photos in Figures 2e and 2f. The drainage event caused water that was being heated by the sun at the surface to drain out underneath the interior ice layer as can be seen in Figure 8 which shows the vertical temperature profiles during the melting phase on Site FLOOD and Site REF. Furthermore, the drainage event appears to have transformed the entire interior ice layer into rotten ice. However, the causal relationship remains uncertain; it is also possible that the formation of the rotten layer allowed the drainage in turn.

Between 30 May and 8 June, the thinning of the interior ice (h_{ii}) at Site REF is non-linear and primarily driven by surface melt (see Figures 3 and 5). Initially, the thinning on Site REF increases but subsequently decreases as the melt progresses. This behavior aligns with the characteristics of non-linear surface sea ice thinning linked to the solid fraction of the material as described by Wiese et al. (2015). Once a material provides a higher solid fraction, thinning decreases.

The linear thinning of the snow ice, as observable in Figure 3, thus fundamentally differs from the thinning of sea ice. A low solid fraction of the snow ice during the melting period would explain this observation.

The thinning of the interior ice at Site FLOOD was clearly influenced by the process of flooding (see Figure 5). Compared to the reference site, the thinning exhibited a reversed non-linear trend: The thinning initially decreases but subsequently increases. It is thus assumed that the solid fraction of the interior ice at the time of melt has been affected by the flooding.

After the drainage event (after 8 June), a "bare" interior ice layer is revealed on Site REF, while the rotten snow ice continued melting on the surface on Site FLOOD forming small melt ponds, some of them aligned in a ring formation with the measurement station as center (Figure 2f)—an observation which is further discussed in Section 4.1.

The bare interior ice layer (after drainage) on Site REF has a significantly higher albedo when compared to Site FLOOD and explains the reversal of trends in albedo evolution after 8 June (see Figure 4). Both sites show the same albedo on 13 June ($\alpha_{d_{FLOOD}} = \alpha_{d_{REF}} = 0.3$) eventually.

Fluctuations in the ocean temperature (Figure 8) correspond well with the tidal calendar. The temperature of the water transported by the tide into the lagoon at a constant depth of 88 cm increased from −1.8°C to 3.4°C between 29 May and 18 June, with an intermediate peak in water temperature of 0°C on 7 June (17:00) caused by the drainage event. After 8 June, the tide also could be seen to heave the ice sheet in the lagoon up and down (see time-lapse video in Hammer et al. (2024a)).

3.4. (f)–(i) Rotting Ice, and Ice Disappearance

This section focuses on the time period after the massive meltwater drainage event on Site REF (8 June) up to the moment the sea ice had fully disappeared on all test sites (20 June). In summary, following main observations have been made between 60 and 71 days after the first flooding:

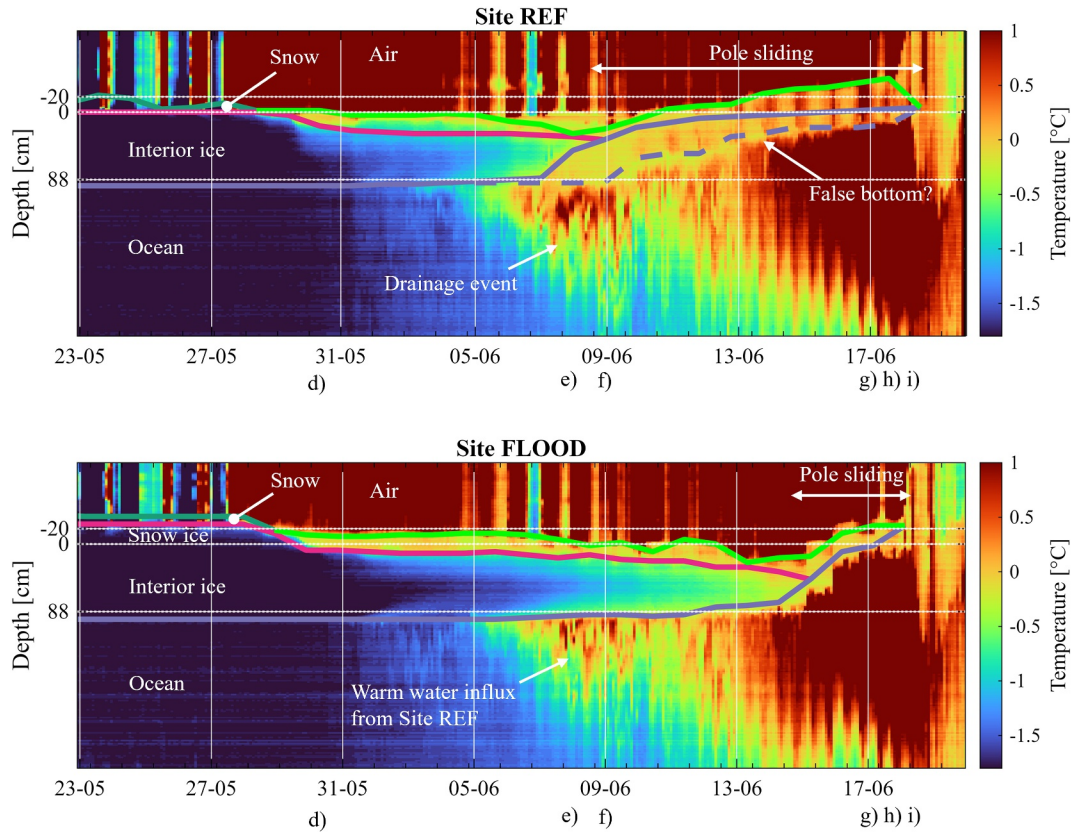

Figure 8. Continuous temperature measurements on Site REF and Site FLOOD showing the period of the drainage event. The dark green lines show the snow surface. The bright green lines show the rotten snow and interior ice (Site REF), and rotten snow ice (Site FLOOD), respectively. The magenta lines show the solid ice top surface. The purple lines show the bottom of the interior ice. The dashed purple line marks either the bottom of the rotten ice or a false bottom formation.

1. The snow ice layer of 26 cm formed by artificial flooding had no significant effect on the moment of the sea ice disappearance.
2. The interior ice on Site REF transformed into a rotten ice layer 6 days before that on Site FLOOD.

Rotting ice starts to cause the measurement pole to sink, creating the impression that the ice sheet "rises" (e.g., Figure 3). It is unclear whether from that point onward the interior ice layer had completely transformed into rotten ice, or if a thin layer of interior ice (with a thickness equal to or smaller than the measurement accuracy) is still present. However, some solid material (i.e., rotten ice) prevented the measurement pole from completely falling over.

Accompanying the sliding of the pole, a melt water trench formed at the edge of the area thickened by flooding on site FLOOD and detached the area from the surrounding landfast ice of the lagoon (Figures 2g and 2h, yellow line). On 19 June, the detached floe started to drift freely for 15 min (Figure 2i) until stopped by remaining landfast ice. Interestingly, the rotten ice layer disappears almost "over night" over a thickness of 50 cm on all sites without any significant thinning beforehand. This rapid disappearance might be explained by the thermocline convection of rotten ice, and/or by the protective role of a false bottom formation, and/or by the high porosity of the rotten ice causing a full collapse of the ice sheet.

Although 26 cm of snow ice on top of 90 cm of interior ice was created by artificial flooding, no significant delay in the ice disappearance on the thickened sites compared to site REF can be observed (see also Table 5) comparing four different measures for determination of sea ice disappearance. This finding seems to be counter-intuitive as it can also be seen that the longevity of the interior ice layer has been extended by 6 days on site FLOOD compared to site REF. However, a layer of rotten ice with a temperature at 0°C (which also prevented the wooden pole from falling over) delayed the full disappearance of the ice on the reference site significantly. The exact timing of the

Table 5
Ice Disappearance Dates at Test Sites Using Four Methods

Site	Camera $\Delta t_{vam} = 0.25hrs$	GPS $\Delta t_{gps} = 2hrs$	Heat cycles $\Delta t_{hc} = 24hrs$	Data logger $\Delta t_{dl} = 0.0833hrs$
REF	20.06.2024–15:14	20.06.2024–17:00	19.06.2024–07:01	18.06.2024–20:35
FLOOD	20.06.2024–13:59[a]	20.06.2024–16:15	19.06.2024–18:16	19.06.2024–00:20
FLOOD1[b]	20.06.2024–09:14	19.06.2024–16:15	19.06.2024–12:16	–
FLOOD2[b]	20.06.2024–07:44	20.06.2024–16:15	21.06.2024–02:16	–

Note. The four methods are: (a) timelapse camera for open water appearance; (b) Snow Ice Mass Balance Apparatus GPS Signal Variability ($>10\sigma$ of first 1,000 hrs) indicating drift onset; (c) thermistor chain heat cycles ceasing (pole fall-over); and (d) data logger failure, with Sentinel-2 imagery distinguishing melt ponds from open water. [a]The ice floe forming at Site FLOOD drifted into the landfast ice on 19 June 2024 at 06:59, which makes this value ambiguous. [b]See Hammer et al. (2024b) for information on these additional test sites.

full disappearance of the sea ice on the test sites can be found in Table 5 comparing four different measures for determination of sea ice disappearance.

4. Discussion

Here we first discuss the results in the context of applying artificial flooding for thickening sea ice with the purpose of extending the sea ice season length. Next, a more engineering focused discussion on the flooding technique is provided, followed by a brief reflection on the comparison of the results to observations from natural flooding.

4.1. Relevance of the Results in the Context of Geoengineering

One of the goals of the field experiment was to investigate the effect of artificial flooding and the creation of snow ice on the summer survival of the sea ice. The common expectation when artificial flooding is discussed in the context of geoengineering is that thicker ice implies extended surface ice presence in summer, with the benefits of higher reflectivity compared to open water. Our field experiment questions this expectation as the additional snow ice layer created (26 cm, 30% thickness increase) did not have any significant effect on the moment of disappearance of the surface sea ice. This result is somewhat counterintuitive as the additional snow ice kept interior ice temperatures low, delaying rotten ice formation by 6 days compared to the reference site. However, the melting behavior of the rotten ice for given boundary conditions at the Vallunden lagoon of limited mechanical stressors, caused surface ice to disappear simultaneously across all sites. An important factor in this simultaneous disappearance is the difference in the thinning of snow ice, interior ice, and rotten ice.

The snow ice thickness decreased with 5.4 mm h^{-1}. The thinning thereby exceeds the growth of 2.3 mm h^{-1}. In contrast to that, the interior ice thickness decreased with a non-linear shape (linearized: 0.8 mm h^{-1}) between 30 May to 8 June. The rotten ice barely thinned but just vanished within a day. No reasonable thinning rate can be provided for the rotten ice. In total 21 days passed between the sea ice surface melt onset (30 May) and the sea ice disappearance, which would result in an averaged thinning of 0.2 mm h^{-1}, which is almost 30 times slower than the thinning rate of the created snow ice.

The Vallunden lagoon is relatively sheltered from mechanical forcing and is therefore not representative of many Arctic sea-ice environments. However, in regions exposed to stronger mechanical stressors, drawing general conclusions from a single field experiment is even more challenging because mechanical processes introduce additional, poorly constrained variables. In such a setting, the rotten ice layer observed at Site REF might have collapsed earlier, for example, through wave-induced mixing into the water column, which would highlight a positive effect of artificial flooding and thickening on summer sea-ice survival.

The test sites were exposed to tidal influxes. The warm water transported reached the two test sites simultaneously ($\Delta t <$ 30 min). The warm water caused basal melting of the bottom interior sea ice. To further discuss the relative importance of basal and surface ablation in the context of our findings, we include findings from Perovich et al. (2011), who explicitly examined melt rates at different Arctic locations. Their results show that, under

comparable heat inputs, basal melt exceeded surface melt: for instance, heat fluxes of 66 and 63 MJm^{-2} produced 0.16 m (surface) and 0.21 m (bottom) melt, and 198 and 207 MJm^{-2} resulted in 0.63 and 0.69 m melt, respectively. These results indicate that sea ice bottom ablation is a more effective mechanism than surface ablation. Consequently, sea ice decline in the Arctic may continue even if the surface layer becomes more resilient to increased solar radiation, if melting from below remains the dominant process. However, for locations governed by surface ablation artificial flooding over a sufficiently large area may have the desired effect of extending the sea ice season as the delay of onset of formation of rotten ice observed in this field trial was significant (Figure 3). Considering the above the results from the present study (tidal influence) cannot simply be generalized for all Arctic sites, but do provide insight on effectiveness for sites exposed to different degrees of surface and basal ablation.

On a similar note it what observed that the massive drainage event and subsequent release of meltwater appear to have contributed to the formation of a false bottom. A false bottom can develop when meltwater drains through channels, accumulates beneath the ice sheet, and refreezes (Salganik et al., 2023). This process heats the interior ice layer from below (increasing basal melt) while simultaneously insulating it from ocean heat fluxes. This protective effect continues until the false bottom is fully ablated through dissolution (Provost et al., 2019). At Site REF, the formation of a false bottom seems plausible due to the observed massive drainage event. However, without in situ measurements to confirm this interpretation, the dashed lines in Figures 3 and 8 could also simply show the bottom layer of the rotten interior ice.

The authors wish to note that in the present study only the basic question of the effect of artificial flooding and snow ice formation *in spring* on local longevity of sea ice was investigated. Imagining that the ice would have been flooded earlier in winter, the relative warming of the interior ice would have been even more severe. When the snow would recover by precipitation or snow drift, as observed during the study, one would decrease the cooling of the interior ice layer by a protective snow ice layer during the cold period. Basal growth could effectively reduce. The flooding in early winter might only be effective if snow layer formation can be prevented or delayed, maximizing the exposure time of the wet surface at cold air temperatures.

It remains unknown to what extend the chosen scale $\left(\sim 1,500\,\mathrm{m}^2\right)$ introduced or negated the influence of boundary effects. On the one hand, the decoupling of the thickened sea ice from the surrounding ice sheet (see Figures 2h and 2i), support the interpretation that this thickened area was not governed by the adjacent ice but rather developed independently at scale. On the other hand, it remains unknown if the formation of circular meltwater trenches around the flooded site itself is caused by scaling effects. Several explanations can be given for why the melt water was collecting in rings around Site FLOOD (Figure 2f). For example, the two rings could be caused by the two consecutive flooding events. The outer ring could also be explained by the formation of an ice volcano, collecting high salt concentrations at the edge, as described by Nakawo and Frederking (1981). The melt water would run off the slope and could create a melt water trench encircling the thickened site as clearly visible in Figure 2g. While it seems unlikely that an ice volcano occurs in a larger scale, the decoupling would be present due to natural features, such as pressure ridges.

Furthermore, the scale of testing was insufficient to investigate the effect of sea ice extent and cloud nucleation on the sea ice disappearance, where latter has a negative correlation according to the findings of Dallósto et al. (2017).

Based on the observations from this study it cannot be concluded at what scale the thickening must be performed to eliminate boundary effects, but perhaps numerical modeling, calibrated on the results of the present study, and other small-scale studies can provide an answer to that question.

Asides from the aspect of sea ice survival there is the aspect of effect of albedo change on reflected solar radiation. A notable observation is the higher albedo at site FLOOD compared to site REF during part of the study period (Figure 4, period e) followed by the inverse during the last part of the study where measurements could be conducted (Figure 4, period f). During the coring of the flooded layer, it was observed that the upper layer of the interior ice would become brighter when the heat or salt (or both) penetrates. The flooding could thus optimize the positive Albedo effect of the ice sheet if the melt water runs off and drained layers are exposed. However, such drained layers also occur when natural first-year sea ice is melting (Light et al., 2015). It remains unknown if and how the drained ice layers after artificial flooding vary in comparison of natural drained surfaces.

The effect on reflected solar radiation depends on further factors of which the cloud cover, for example, is a very important one. For the field experiment conducted we account for these specific conditions utilizing the Global Warming Potential (GWP) framework, despite its limitations in directly applying it to the scenario of the field experiment which we acknowledge (Bright & Lund, 2021). In short, the GWP is a metric used to compare the ability of different greenhouse gases to trap heat in the atmosphere over a specific time horizon, and relative to carbon dioxide (CO_2). The $GWP_{\Delta\alpha}$(TH) thus gives the GWP for a change in albedo ($\Delta\alpha$) based on a specific temporal accumulation or metric time horizon (TH; i.e.; years) and the cumulative change in radiative forcing $\Delta\alpha_d$. TH for 100 years would thus provide a normalized WP effect accumulating for 100 years. Values of $GWP_{\Delta\alpha}$(TH) based on observed change of albedo in the present study for TH equal to 1, 20, 50, and 100 years are in the order of −0.2, −0.025, −0.01, and −0.005 kg CO_2-eq m^{-2}, respectively. A choice for a relevant time horizon to assess the impact of measures like flooding in the context of geoengineering is a policy makers decision and not further discussed here. The values presented thus show a positive impact given the weather conditions during the experiment (i.e., negative value), however these do not yet account for the emissions required for execution of the flooding. For a 100-year horizon the obtained magnitudes are, for example, in the same order as the CO_2 emissions of only the fuel consumed by the pumps (about +0.004 kgCO_2 m^{-2}), where most emissions are of course associated with transport to and from the locations of the flood pumps which the scale of flooding would have to then compensate for.

The authors finally wish to note that other equally relevant aspects of geoengineering techniques in the Arctic require further proper consideration (e.g., biological processes, chemical processes, regional impacts) to make a holistically informed decision on such interventions. The same holds for the application of flooding for purposes different from delaying the disappearance of ice in summer, such as local avoidance of coastal erosion and protection of villages and infrastructure, raising the surface albedo, and/or cooling the surface.

This experiment does demonstrate that it is not just sufficient to create thicker ice. The challenge in relation to artificial flooding is in understanding the thinning process associated with the ice created by specific flooding strategies.

4.2. Considerations With Respect to the Flooding Technique

Accepting that the snow cannot be removed prior to flooding on a large scale, it seems most effective to flood the full snow layer at once, creating a snow ice layer, and adding thinner water layers (i.e., water lifting) continuously afterward. In our field experiment we thus flooded a 20 cm water column with the aim to flood the full snow layer, creating a wet surface in interaction with the air to maximize heat exchange between flooded water and air. This mechanism was found to be of most importance when comparing the results of the freezing effectiveness between 5 and 20 mm thick water layers on the interior sheet by Szilder and Lozowski (1989). However, in the present study, water during the second flooding event simply ran off the created smooth snow ice surface, starting to flood the surrounding snow layer again, causing the contact time of the wet surface in interaction with the air to be low. Also, there seems to exist an upper limit of thickening for which the heat loss to the atmosphere is the most dominating factor. For example, a flooding layer of 80–100 mm thickness would delay the heat transfer into the interior ice and thus freezing, as the full interior ice would warm up significantly (Adams et al., 1960). Thus, the effectiveness of the thickening is dependent on the duration, and amount of flooding.

Note that most of the numerical studies on the application of artificial flooding for the purpose of geoengineering consider a continuous wet surface between the flooded water and air (Desch et al., 2017; Zampieri & Goessling, 2019) thus maximizing ice formation. Only Pauling and Bitz (2021) considered the problem of flooding snow layers by allowing the mixture of snow and flooded water to freeze, focusing on the timing of flooding of the snow as main driver for sea ice thickening in their simulations. However, also here the geophysical distinction between snow ice and sea ice is missing, and the effect of snow drift is not considered. Thus, the flooded layer is instantly turned into a layer of ice, with a salinity depending on the snow/sea water ratio. The layer is at freezing temperature, and freezing processes of the slush layer are neglected.

4.3. Comparison of Natural Flooding and Artificial Flooding

The impossibility to remove snow at a large scale makes the application of artificial flooding for sea ice thickening in the context of geoengineering to be comparable of natural flooding events. Numerical modeling and upscaled analyses of artificial flooding are thus often based on knowledge derived from natural flooding. For future

modeling it is thus essential to highlight the main differences of artificial flooding for the purpose of sea ice thickening or enhancing the longevity of the ice (i.e., global scale) and natural flooding. In case of artificial flooding the:

- thickening happens at positive freeboard
- full snow layer is flooded (wet surface)
- creation of a hydrostatic reservoir has to be accounted for
- surface albedo/layer changes (e.g., wet surface, snow recovery)

Artificial flooding is performed at a positive freeboard, which can lead to the formation of ice volcanoes and associated effects like water run-off, and meltwater trench formation as observed in the present study, or salt accumulation at the edges of the ice volcano as observed by Nakawo and Frederking (1981). Unlike natural flooding, artificial flooding generates significant hydrostatic pressure, which may influence the critical permeability temperature formulated by Golden (2001). The authors assume that brine can effectively penetrate the interior ice at lower temperatures. Although the extent depends on the flooding approach, the entire snow layer will eventually become flooded, something that typically does not occur in natural flooding events.

Despite all differences, the flooding and slush formation of the present campaign resembled that of a natural flooding event as documented by Provost et al. (2017): After a big storm and break-up event of an ice floe in the Arctic on 17 February 2015, the lower snow layer on the floe was partially flooded and 25 cm of slush formed in 3 hrs. The low initial temperatures of the ice (ice temperature profile from −2°C to −17°C) and a cold spell (i.e., −20°C on February 18) formed a snow ice layer of 10 cm within 2–4 days (i.e., 2 mm h^{-1} and 1 mm h^{-1}) despite the insulating effect of the snow. Interestingly, a similar growth rate (i.e., 2.3 mm h^{-1} has been observed in the present study). Further, the flooding observed by Provost et al. (2017) increased the temperature of the interior ice by roughly 3°C in a natural flooding event. In the present study, the water increased the temperature of the interior ice temperature by 2.3–2.7°C in average over the full thickness and up to 5.9°C at the ice surface.

5. Conclusion

This study investigated the impact of artificial flooding on the growth and melting of snow-covered first-year sea ice. Artificial flooding has been gaining attention as a geoengineering method being proposed in broad literature as a means to delay the disappearance of sea ice during the summer. Field experiments conducted in the Vallunden lagoon on Spitsbergen in the Arctic revealed that application of artificial flooding for an area of $\sim 1,500\,m^2$ altered the interior ice temperature profile, affecting its permeability and thus leading to the intrusion of a high-saline liquid into the underlying interior ice layer. The additional snow ice layer created by flooding (and freezing) delayed the underlying interior ice from transformation into rotten ice early in the summer season. The albedo evolution of the ice surface was influenced as revealed by events such as slush formation, snow drift, and or meltwater drainage. The findings of this study highlight the geophysical interplay between snow insulation, slush formation, ice permeability, salt migration, nonlinear sea ice thinning, and drainage events. For the location, scale, and timing under which this field experiment was executed the artificial flooding and subsequent growth of a 26 cm thick layer of snow ice on top of 90 cm of natural sea ice did not delay the disappearance of the ice in summer. The results do provide indications that for locations with limited bottom ablation and/or increased mechanical stressors summer ice disappearance may be delayed.

Appendix A: Methodical Problems

During the last phase of the experiments, the pole did not only sink vertically into the rotten ice, but also began to tilt. As a result, data from the radiometers were only used up until 13 June. This was the last day where the tilt of the radiometer on site FLOOD was minor and the daily mean incident short wave radiation for site REF and FLOOD did not show a major difference indicative of measurement error (i.e., tilting of one of the poles the devices were attached to).

The formation of an ice bustle (ice formation attached to the measurement station due to water level variation) during the depletion phase of the reservoir complicated the application of "regular" layer detection methods by SIMBA. The ice bustles had gathered snow in close approximation to the real snow cover, which made an automatized snow layer distinction as provided by Liao et al. (2019) impossible.

Several algorithms for automatized layer detection have been implemented during the data analysis but showed unreliable when applied for analysis of the data during the flooding and melting phase and thus have not been shown here. This finding is not surprising as most of the algorithms are developed for application on steady state conditions and linearly sorted isotherms with hard-coded thresholds for natural flooding events (Cheng et al., 2020; Liao et al., 2019). But even a more robust detection algorithm as provided by Plante et al. (2024) did not give proper results in this application due to the layering of slush and snow ice after flooding. The authors of the present study thus determined the layers manually with the help of the diffusivity proxy (e.g., Figure 3) and vertical temperature gradient (i.e., air, snow) which can be found in Supporting Information S1. Hopefully, the gathered data can be used to create robust layer detection for artificially flooded ice in the future.

Conflict of Interest

The authors declare no conflicts of interest relevant to this study.

Availability Statement

The data are available at 4TU (https://data.4tu.nl/datasets/dae61d9b-d079-4959-868e-591b7de1b7f6) (Hammer et al., 2024a), with additional data set details in Hammer et al. (2024b).

Acknowledgments
We wish to thank the University Centre of Svalbard (UNIS) and the TU Delft Climate Action Program for supporting this research. The analysis presented in this paper is based on a public dataset which was collected as part of a collaboration between Arctic Reflections, TU Delft, and UNIS. We wish to thank Fonger Ypma and Tom Meijeraan (Arctic Reflections) for all their efforts and contributions to funding, organizing, and execution of the data collection campaign and spending the time together in Svea. Arctic Reflections have previously released a report with their analysis of the data (Arctic Reflections, 2024). We acknowledge the government of Svalbard for permission to conduct the field experiments in the Vallunden lagoon.

References

Ackley, S. F., Perovich, D. K., Maksym, T., Weissling, B., & Xie, H. (2020). Surface flooding of Antarctic summer sea ice. *Annals of Glaciology*, *61*(82), 117–126. https://doi.org/10.1017/aog.2020.22

Adams, C. M., French, D. N., & Kingery, W. D. (1960). Solidification of sea ice. *Journal of Glaciology*, *3*(28), 745–761. https://doi.org/10.3189/s0022143000018050

Arctic Reflections. (2024). Svalbard Field Test. Research summary report September 20th, 2024 [PDF file]. Retrieved from https://docsend.com/view/dhvkc67yc4bfpfds

Barrette, P. D. (2015). Overview of ice roads in Canada: Design, usage and climate change adaptation. In *Technical report (National research council of Canada. Ocean, coastal and River engineering); no. OCRE-TR-2015-011*. https://doi.org/10.4224/40000400

Baudais, D. J., Watts, J. S., & Masterson, D. M. (1976). A system for offshore drilling in the Arctic Islands. In *Proceedings of the annual offshore technology conference, 1976-May* (pp. 31–44). https://doi.org/10.4043/2622-ms

Bright, R. M., & Lund, M. T. (2021). CO_2-equivalence metrics for surface albedo change based on the radiative forcing concept: A critical review. *Atmospheric Chemistry and Physics*, *21*(12), 9887–9907. https://doi.org/10.5194/acp-21-9887-2021

Cheng, Y., Cheng, B., Zheng, F., Vihma, T., Kontu, A., Yang, Q., & Liao, Z. (2020). Air/snow, snow/ice and ice/water interfaces detection from high-resolution vertical temperature profiles measured by ice mass-balance buoys on an Arctic lake. *Annals of Glaciology*, *61*(83), 309–319. https://doi.org/10.1017/aog.2020.51

Cox, G. F. (1979). Artificial ice islands for exploratory drilling. In *Proceedings of the 5th port and ocean engineering under arctic conditions* (pp. 147–162).

Dallósto, M., Beddows, D. C., Tunved, P., Krejci, R., Ström, J., Hansson, H. C., et al. (2017). Arctic sea ice melt leads to atmospheric new particle formation. *Scientific Reports*, *7*(1), 3318. https://doi.org/10.1038/s41598-017-03328-1

Desch, S. J., Smith, N., Groppi, C., Vargas, P., Jackson, R., Kalyaan, A., et al. (2017). Arctic ice management. *Earth's Future*, *5*(1), 107–127. https://doi.org/10.1002/2016EF000410

Eicken, H., Fischer, H., & Lemke, P. (1995). Effects of the snow cover on Antarctic sea ice and potential modulation of its response to climate change. *Annals of Glaciology*, *21*, 369–376. https://doi.org/10.3189/s0260305500016086

Fichefet, T., & Morales Maqueda, M. A. (1999). Modelling the influence of snow accumulation and snow-ice formation on the seasonal cycle of the Antarctic sea-ice cover. *Climate Dynamics*, *15*(4), 251–268. https://doi.org/10.1007/s003820050280

Field, L., Ivanova, D., Bhattacharyya, S., Mlaker, V., Sholtz, A., Decca, R., et al. (2018). Increasing Arctic sea ice Albedo using localized reversible geoengineering. *Earth's Future*, *6*(6), 882–901. https://doi.org/10.1029/2018EF000820

Gilbert, E., & Holmes, C. (2024). 2023's Antarctic sea ice extent is the lowest on record. *Weather*, *79*(2), 46–51. https://doi.org/10.1002/wea.4518

Golden, K. M. (2001). Brine percolation and the transport properties of sea ice. *Annals of Glaciology*, *33*, 28–36. https://doi.org/10.3189/172756401781818329

Haas, C., Thomas, D. N., & Bareiss, J. (2001). Surface properties and processes of perennial Antarctic sea ice in summer. *Journal of Glaciology*, *47*(159), 1–13. https://doi.org/10.3189/172756501781831864

Hammer, T. C., Shestov, A., van Dijke, L., Ypma, F., Meijeraan, T., & Hendrikse, H. (2024a). Data from field experiments on artificial flooding and thickening of snow-covered first-year sea ice and the melting of thickened ice. *4TU.ResearchData. dataset*. Retrieved from https://data.4tu.nl/datasets/dae61d9b-d079-4959-868e-591b7de1b7f6

Hammer, T. C., Shestov, A., van Dijke, L. L., Ypma, F., Meijeraan, T., & Hendrikse, H. (2024b). Field data on sea ice restoration by artificial flooding. *Data in Brief*, *57*, 111117. https://doi.org/10.1016/j.dib.2024.111117

Itkin, P., Spreen, G., Cheng, B., Doble, M., Girard-Ardhuin, F., Haapala, J., et al. (2017). Thin ice and storms: Sea ice deformation from buoy arrays deployed during N-ICE2015. *Journal of Geophysical Research: Oceans*, 6394–6415. https://doi.org/10.1002/2016JC012403

Jackson, K., Wilkinson, J., Maksym, T., Meldrum, D., Beckers, J., Haas, C., & Mackenzie, D. (2013). A novel and low-cost sea ice mass balance buoy. *Journal of Atmospheric and Oceanic Technology*, *30*(11), 2676–2688. https://doi.org/10.1175/JTECH-D-13-00058.1

Jutras, M., Vancoppenolle, M., Lourenço, A., Vivier, F., Carnat, G., Madec, G., et al. (2016). Thermodynamics of slush and snow–ice formation in the Antarctic sea-ice zone. *Deep-Sea Research Part II Topical Studies in Oceanography*, *131*, 75–83. https://doi.org/10.1016/j.dsr2.2016.03.008

Karelov, A., Shkhinek, K., & Belyaev, N. (2015). Using of ice for constructing Islands in the Arctic conditions. *Applied Mechanics and Materials*, *725–726*, 245–250. https://doi.org/10.4028/www.scientific.net/amm.725-726.245

Kopp, G. (2023). Daily solar flux as a function of latitude and time. *Solar Energy*, *249*(August 2022), 250–254. https://doi.org/10.1016/j.solener.2022.11.022

Ledley, T. S. (1991). Snow on sea ice: Competing effects in shaping climate. *Journal of Geophysical Research*, *96*(D9), 17195–17208. https://doi.org/10.1029/91jd01439

Lewis, M. J., Tison, J. L., Weissling, B., Delille, B., Ackley, S. F., Brabant, F., & Xie, H. (2011). Sea ice and snow cover characteristics during the winter-spring transition in the Bellingshausen Sea: An overview of SIMBA 2007. *Deep-Sea Research Part II Topical Studies in Oceanography*, *58*(9–10), 1019–1038. https://doi.org/10.1016/j.dsr2.2010.10.027

Liao, Z., Cheng, B., Zhao, J. C., Vihma, T., Jackson, K., Yang, Q., et al. (2019). Snow depth and ice thickness derived from SIMBA ice mass balance buoy data using an automated algorithm. *International Journal of Digital Earth*, *12*(8), 962–979. https://doi.org/10.1080/17538947.2018.1545877

Light, B., Perovich, D. K., Webster, M. A., Polashenski, C., & Dadic, R. (2015). Optical properties of melting first-year Arctic sea ice. *Journal of Geophysical Research: Oceans*, *120*, 1–17. https://doi.org/10.1002/2015JC011163

Lytle, V. I., & Ackley, S. F. (1996). Heat flux through sea ice in the western Weddell Sea: Convective and conductive transfer processes. *Journal of Geophysical Research*, *101*(C4), 8853–8868. https://doi.org/10.1029/95JC03675

Maksym, T., & Jeffries, M. O. (2001). Phase and compositional evolution of the flooded layer during snow-ice formation on Antarctic sea ice. *Annals of Glaciology*, *33*(3), 37–44. https://doi.org/10.3189/172756401781818860

Manninen, T., Anttila, K., Jääskeläinen, E., Riihelä, A., Peltoniemi, J., Räisänen, P., et al. (2021). Effect of small-scale snow surface roughness on snow albedo and reflectance. *The Cryosphere*, *15*(2), 793–820. https://doi.org/10.5194/tc-15-793-2021

Massom, R. A., Drinkwater, M. R., & Haas, C. (1997). Winter snow cover on sea ice in the Weddell Sea. *Journal of Geophysical Research*, *102*(1), 1101–1117. https://doi.org/10.1029/96jc02992

Massom, R. A., Eicken, H., Jeffries, O., Drinkwater, M. R., Worby, P., Lytle, I., et al. (2001). Snow on Antarctic sea ice. *Reviews of Geophysics*, *39*(2000), 413–445. https://doi.org/10.1029/2000RG000085

Masterson, D. M. (2009). State of the art of ice bearing capacity and ice construction. *Cold Regions Science and Technology*, *58*(3), 99–112. https://doi.org/10.1016/j.coldregions.2009.04.002

Meguro, H. (1962). Plankton ice in Antarctic Ocean. Antarctic record 14 1192–1199.

Morozov, E. G., Marchenko, A. V., Filchuk, K. V., Kowalik, Z., Marchenko, N. A., & Ryzhov, I. V. (2019). Sea ice evolution and internal wave generation due to a tidal jet in a frozen sea. *Applied Ocean Research*, *87*(October 2018), 179–191. https://doi.org/10.1016/j.apor.2019.03.024

Nakawo, M., & Frederking, R. (1981). *The salinity of artificial built-up ice made by successive floodings of sea water*. National Research Council Canada, Division of Building Research.

Pauling, A. G., & Bitz, C. M. (2021). Arctic sea ice response to flooding of the snow layer in future warming scenarios. *Earth's Future*, *9*(10). https://doi.org/10.1029/2021EF002136

Perovich, D. K., Elder, B. C., Claffey, K. J., Stammerjohn, S., Smith, R., Ackley, S. F., et al. (2004). Winter sea-ice properties in Marguerite Bay, Antarctica. *Deep-Sea Research Part II Topical Studies in Oceanography*, *51*(17–19), 2023–2039. https://doi.org/10.1016/j.dsr2.2004.07.024

Perovich, D. K., Richter-Menge, J. A., Jones, K. F., Light, B., Elder, B. C., Polashenski, C., et al. (2011). Arctic sea-ice melt in 2008 and the role of solar heating. *Annals of Glaciology*, *52*(57), 355–359. https://doi.org/10.3189/172756411795931714

Plante, M., Lemieux, J.-f., Tremblay, L. B., Tivy, A., Angnatok, J., Roy, F., et al. (2024). Using Icepack to reproduce ice mass balance buoy observations in landfast ice: Improvements from the mushy-layer thermodynamics (pp. 1685–1708). https://doi.org/10.5194/tc-18-1685-2024

Provost, C., Sennéchael, N., Miguet, J., Itkin, P., Rösel, A., Koenig, Z., et al. (2017). Observations of flooding and snow-ice formation in a thinner Arctic sea-ice regime during the N-ICE2015 campaign: Influence of basal ice melt and storms. *Journal of Geophysical Research: Oceans*, 6394–6415. https://doi.org/10.1002/2016JC012011

Provost, C., Sennéchael, N., & Sirven, J. (2019). Contrasted summer processes in the sea ice for two neighboring floes north of 84°N: Surface and basal melt and false bottom Formation. *Journal of Geophysical Research: Oceans*, *124*(6), 3963–3986. https://doi.org/10.1029/2019JC015000

Rösel, A., Itkin, P., King, J., Divine, D., Wang, C., Granskog, M. A., et al. (2018). Thin sea ice, thick snow, and widespread negative freeboard observed during N-ICE2015 north of Svalbard. *Journal of Geophysical Research: Oceans*, *123*(2), 1156–1176. https://doi.org/10.1002/2017JC012865

Salganik, E., Katlein, C., Lange, B. A., Matero, I., Lei, R., Fong, A. A., et al. (2023). Temporal evolution of under-ice meltwater layers and false bottoms and their impact on summer Arctic sea ice mass balance. https://doi.org/10.1525/elementa.2022.00035

Saloranta, T. M. (2000). Modeling the evolution of snow, snow ice and ice in the Baltic Sea. *Tellus, Series A: Dynamic Meteorology and Oceanography*, *52*(1), 93–108. https://doi.org/10.3402/tellusa.v52i1.12255

Siegert, M., Sevestre, H., Bentley, M. J., Brigham-Grette, J., Burgess, H., Buzzard, S., et al. (2025). Safeguarding the polar regions from dangerous geoengineering: A critical assessment of proposed concepts and future prospects. *Frontiers in Science*, *3*, 1527393. https://doi.org/10.3389/fsci.2025.1527393

Szilder, K., & Lozowski, E. P. (1989). Optimizing the growth thermodynamics of artificial floating ice platforms. *Ocean Engineering*, *16*(1), 99–115. https://doi.org/10.1016/0029-8018(89)90045-0

Takizawa, T. (1985). Salination of snow on sea ice and formation of snow ice. *Annals of Glaciology*, *6*, 309–310. https://doi.org/10.3189/1985aog6-1-309-310

Webster, M. A., & Warren, S. G. (2022). Regional geoengineering using tiny glass bubbles would accelerate the loss of Arctic sea ice. *Earth's Future*, *10*(10). https://doi.org/10.1029/2022EF002815

Wiese, M., Griewank, P., & Notz, D. (2015). On the thermodynamics of melting sea ice versus melting freshwater ice. *Annals of Glaciology*, *56*(69), 191–199. https://doi.org/10.3189/2015AoG69A874

Yadav, J., Kumar, A., & Mohan, R. (2020). Dramatic decline of Arctic sea ice linked to global warming. *Natural Hazards*, *103*(2), 2617–2621. https://doi.org/10.1007/s11069-020-04064-y

Zampieri, L., & Goessling, H. F. (2019). Sea ice targeted geoengineering can delay Arctic sea ice decline but not global warming. *Earth's Future*, *7*(12), 1296–1306. https://doi.org/10.1029/2019EF001230